BABAR-PUB-18/010
SLAC-PUB-17455

Search for $B^- \to \Lambda\bar{p}\nu\bar{\nu}$ with the *BABAR* experiment

J. P. Lees, V. Poireau, and V. Tisserand
Laboratoire d'Annecy-le-Vieux de Physique des Particules (LAPP), Université de Savoie, CNRS/IN2P3, F-74941 Annecy-Le-Vieux, France

E. Grauges
Universitat de Barcelona, Facultat de Fisica, Departament ECM, E-08028 Barcelona, Spain

A. Palano
INFN Sezione di Bari and Dipartimento di Fisica, Università di Bari, I-70126 Bari, Italy

G. Eigen
University of Bergen, Institute of Physics, N-5007 Bergen, Norway

D. N. Brown and Yu. G. Kolomensky
Lawrence Berkeley National Laboratory and University of California, Berkeley, California 94720, USA

M. Fritsch, H. Koch, and T. Schroeder
Ruhr Universität Bochum, Institut für Experimentalphysik 1, D-44780 Bochum, Germany

R. Cheaib[b], C. Hearty[ab], T. S. Mattison[b], J. A. McKenna[b], and R. Y. So[b]
Institute of Particle Physics[a]; University of British Columbia[b], Vancouver, British Columbia, Canada V6T 1Z1

V. E. Blinov[abc], A. R. Buzykaev[a], V. P. Druzhinin[ab], V. B. Golubev[ab], E. A. Kozyrev[ab], E. A. Kravchenko[ab], A. P. Onuchin[abc], S. I. Serednyakov[ab], Yu. I. Skovpen[ab], E. P. Solodov[ab], and K. Yu. Todyshev[ab]
Budker Institute of Nuclear Physics SB RAS, Novosibirsk 630090[a], Novosibirsk State University, Novosibirsk 630090[b], Novosibirsk State Technical University, Novosibirsk 630092[c], Russia

A. J. Lankford
University of California at Irvine, Irvine, California 92697, USA

B. Dey, J. W. Gary, and O. Long
University of California at Riverside, Riverside, California 92521, USA

A. M. Eisner, W. S. Lockman, and W. Panduro Vazquez
University of California at Santa Cruz, Institute for Particle Physics, Santa Cruz, California 95064, USA

D. S. Chao, C. H. Cheng, B. Echenard, K. T. Flood, D. G. Hitlin, J. Kim, Y. Li, T. S. Miyashita, P. Ongmongkolkul, F. C. Porter, and M. Röhrken
California Institute of Technology, Pasadena, California 91125, USA

Z. Huard, B. T. Meadows, B. G. Pushpawela, M. D. Sokoloff, and L. Sun*
University of Cincinnati, Cincinnati, Ohio 45221, USA

J. G. Smith and S. R. Wagner
University of Colorado, Boulder, Colorado 80309, USA

D. Bernard and M. Verderi
Laboratoire Leprince-Ringuet, Ecole Polytechnique, CNRS/IN2P3, F-91128 Palaiseau, France

D. Bettoni[a], C. Bozzi[a], R. Calabrese[ab], G. Cibinetto[ab], E. Fioravanti[ab], I. Garzia[ab], E. Luppi[ab], and V. Santoro[a]
INFN Sezione di Ferrara[a]; Dipartimento di Fisica e Scienze della Terra, Università di Ferrara[b], I-44122 Ferrara, Italy

A. Calcaterra, R. de Sangro, G. Finocchiaro, S. Martellotti,
P. Patteri, I. M. Peruzzi, M. Piccolo, M. Rotondo, and A. Zallo
INFN Laboratori Nazionali di Frascati, I-00044 Frascati, Italy

S. Passaggio and C. Patrignani[†]
INFN Sezione di Genova, I-16146 Genova, Italy

H. M. Lacker
Humboldt-Universität zu Berlin, Institut für Physik, D-12489 Berlin, Germany

B. Bhuyan
Indian Institute of Technology Guwahati, Guwahati, Assam, 781 039, India

U. Mallik
University of Iowa, Iowa City, Iowa 52242, USA

C. Chen, J. Cochran, and S. Prell
Iowa State University, Ames, Iowa 50011, USA

A. V. Gritsan
Johns Hopkins University, Baltimore, Maryland 21218, USA

N. Arnaud, M. Davier, F. Le Diberder, A. M. Lutz, and G. Wormser
Laboratoire de l'Accélérateur Linéaire, IN2P3/CNRS et Université Paris-Sud 11, Centre Scientifique d'Orsay, F-91898 Orsay Cedex, France

D. J. Lange and D. M. Wright
Lawrence Livermore National Laboratory, Livermore, California 94550, USA

J. P. Coleman, E. Gabathuler,[‡] D. E. Hutchcroft, D. J. Payne, and C. Touramanis
University of Liverpool, Liverpool L69 7ZE, United Kingdom

A. J. Bevan, F. Di Lodovico, and R. Sacco
Queen Mary, University of London, London, E1 4NS, United Kingdom

G. Cowan
University of London, Royal Holloway and Bedford New College, Egham, Surrey TW20 0EX, United Kingdom

Sw. Banerjee, D. N. Brown, and C. L. Davis
University of Louisville, Louisville, Kentucky 40292, USA

A. G. Denig, W. Gradl, K. Griessinger, A. Hafner, and K. R. Schubert
Johannes Gutenberg-Universität Mainz, Institut für Kernphysik, D-55099 Mainz, Germany

R. J. Barlow[§] and G. D. Lafferty
University of Manchester, Manchester M13 9PL, United Kingdom

R. Cenci, A. Jawahery, and D. A. Roberts
University of Maryland, College Park, Maryland 20742, USA

R. Cowan
Massachusetts Institute of Technology, Laboratory for Nuclear Science, Cambridge, Massachusetts 02139, USA

S. H. Robertson[ab] and R. M. Seddon[b]

Institute of Particle Physics[a]; McGill University[b], Montréal, Québec, Canada H3A 2T8

N. Neri[a] and F. Palombo[ab]
INFN Sezione di Milano[a]; Dipartimento di Fisica, Università di Milano[b], I-20133 Milano, Italy

L. Cremaldi, R. Godang,[¶] and D. J. Summers
University of Mississippi, University, Mississippi 38677, USA

P. Taras
Université de Montréal, Physique des Particules, Montréal, Québec, Canada H3C 3J7

G. De Nardo and C. Sciacca
INFN Sezione di Napoli and Dipartimento di Scienze Fisiche, Università di Napoli Federico II, I-80126 Napoli, Italy

G. Raven
NIKHEF, National Institute for Nuclear Physics and High Energy Physics, NL-1009 DB Amsterdam, The Netherlands

C. P. Jessop and J. M. LoSecco
University of Notre Dame, Notre Dame, Indiana 46556, USA

K. Honscheid and R. Kass
Ohio State University, Columbus, Ohio 43210, USA

A. Gaz[a], M. Margoni[ab], M. Posocco[a], G. Simi[ab], F. Simonetto[ab], and R. Stroili[ab]
INFN Sezione di Padova[a]; Dipartimento di Fisica, Università di Padova[b], I-35131 Padova, Italy

S. Akar, E. Ben-Haim, M. Bomben, G. R. Bonneaud, G. Calderini, J. Chauveau, G. Marchiori, and J. Ocariz
Laboratoire de Physique Nucléaire et de Hautes Energies, Sorbonne Université, Paris Diderot Sorbonne Paris Cité, CNRS/IN2P3, F-75252 Paris, France

M. Biasini[ab], E. Manoni[a], and A. Rossi[a]
INFN Sezione di Perugia[a]; Dipartimento di Fisica, Università di Perugia[b], I-06123 Perugia, Italy

G. Batignani[ab], S. Bettarini[ab], M. Carpinelli[ab],[**] G. Casarosa[ab], M. Chrzaszcz[a], F. Forti[ab], M. A. Giorgi[ab], A. Lusiani[ac], B. Oberhof[ab], E. Paoloni[ab], M. Rama[a], G. Rizzo[ab], J. J. Walsh[a], and L. Zani[ab]
INFN Sezione di Pisa[a]; Dipartimento di Fisica, Università di Pisa[b]; Scuola Normale Superiore di Pisa[c], I-56127 Pisa, Italy

A. J. S. Smith
Princeton University, Princeton, New Jersey 08544, USA

F. Anulli[a], R. Faccini[ab], F. Ferrarotto[a], F. Ferroni[a],[††] A. Pilloni[ab], and G. Piredda[a‡]
INFN Sezione di Roma[a]; Dipartimento di Fisica, Università di Roma La Sapienza[b], I-00185 Roma, Italy

C. Bünger, S. Dittrich, O. Grünberg, M. Heß, T. Leddig, C. Voß, and R. Waldi
Universität Rostock, D-18051 Rostock, Germany

T. Adye and F. F. Wilson
Rutherford Appleton Laboratory, Chilton, Didcot, Oxon, OX11 0QX, United Kingdom

S. Emery and G. Vasseur
IRFU, CEA, Université Paris-Saclay, F-91191 Gif-sur-Yvette, France

D. Aston, C. Cartaro, M. R. Convery, J. Dorfan, W. Dunwoodie, M. Ebert, R. C. Field, B. G. Fulsom, M. T. Graham, C. Hast, W. R. Innes,[‡] P. Kim, D. W. G. S. Leith, S. Luitz, D. B. MacFarlane, D. R. Muller, H. Neal, B. N. Ratcliff, A. Roodman, M. K. Sullivan, J. Va'vra, and W. J. Wisniewski

SLAC National Accelerator Laboratory, Stanford, California 94309 USA

M. V. Purohit and J. R. Wilson
University of South Carolina, Columbia, South Carolina 29208, USA

A. Randle-Conde and S. J. Sekula
Southern Methodist University, Dallas, Texas 75275, USA

H. Ahmed
St. Francis Xavier University, Antigonish, Nova Scotia, Canada B2G 2W5

M. Bellis, P. R. Burchat, and E. M. T. Puccio
Stanford University, Stanford, California 94305, USA

M. S. Alam and J. A. Ernst
State University of New York, Albany, New York 12222, USA

R. Gorodeisky, N. Guttman, D. R. Peimer, and A. Soffer
Tel Aviv University, School of Physics and Astronomy, Tel Aviv, 69978, Israel

S. M. Spanier
University of Tennessee, Knoxville, Tennessee 37996, USA

J. L. Ritchie and R. F. Schwitters
University of Texas at Austin, Austin, Texas 78712, USA

J. M. Izen and X. C. Lou
University of Texas at Dallas, Richardson, Texas 75083, USA

F. Bianchi[ab], F. De Mori[ab], A. Filippi[a], and D. Gamba[ab]
INFN Sezione di Torino[a]; Dipartimento di Fisica, Università di Torino[b], I-10125 Torino, Italy

L. Lanceri and L. Vitale
INFN Sezione di Trieste and Dipartimento di Fisica, Università di Trieste, I-34127 Trieste, Italy

F. Martinez-Vidal and A. Oyanguren
IFIC, Universitat de Valencia-CSIC, E-46071 Valencia, Spain

J. Albert[b], A. Beaulieu[b], F. U. Bernlochner[b], G. J. King[b], R. Kowalewski[b], T. Lueck[b], I. M. Nugent[b], J. M. Roney[b], R. J. Sobie[ab], and N. Tasneem[b]
Institute of Particle Physics[a]; University of Victoria[b], Victoria, British Columbia, Canada V8W 3P6

T. J. Gershon, P. F. Harrison, and T. E. Latham
Department of Physics, University of Warwick, Coventry CV4 7AL, United Kingdom

R. Prepost and S. L. Wu
University of Wisconsin, Madison, Wisconsin 53706, USA

We search for the rare flavor-changing neutral current process $B^- \to \Lambda\bar{p}\nu\bar{\nu}$ using data from the *BABAR* experiment. A total of 424 fb^{-1} of e^+e^- collision data collected at the center-of-mass energy of the $\Upsilon(4S)$ resonance is used in this study, corresponding to a sample of $(471 \pm 3) \times 10^6$ $B\overline{B}$ pairs. Signal $B^- \to \Lambda\bar{p}\nu\bar{\nu}$ candidates are identified by first fully reconstructing a B^+ decay in one of many possible exclusive decays to hadronic final states, then examining detector activity that is not associated with this reconstructed B^+ decay for evidence of a signal $B^- \to \Lambda\bar{p}\nu\bar{\nu}$ decay. The data yield is found to be consistent with the expected background contribution under a null signal hypothesis, resulting in an upper limit of $\mathcal{B}(B^- \to \Lambda\bar{p}\nu\bar{\nu}) < 3.0 \times 10^{-5}$ at the 90% confidence level.

PACS numbers: 13.20.He, 12.38.Qk, 14.40.Nd

Flavor-changing neutral current (FCNC) processes are suppressed in the standard model (SM) of particle interactions due to their absence at tree level, appearing first at one-loop level. Consequently, they are an excellent place to look for evidence of new physics contributions, as heavy mediators could also occur in these loop processes, resulting in potentially measurable deviations from SM predictions. The process $B^- \to \Lambda\overline{p}\nu\overline{\nu}$ (*CP* conjugate processes are implied here and throughout this paper) is the baryonic analog of $B \to K^{(*)}\nu\overline{\nu}$, occurring in the SM via a FCNC $b \to s\nu\overline{\nu}$ transition through Z-penguin or W-box processes. In the case of $B^- \to \Lambda\overline{p}\nu\overline{\nu}$, two $q\overline{q}$ pairs are produced from the vacuum to yield the Λ and $\overline{p}$ in the final state (see Fig. 1). The branching fraction is predicted to be $\mathcal{B}(B^- \to \Lambda\overline{p}\nu\overline{\nu}) = (7.9 \pm 1.9) \times 10^{-7}$ [1].

Although the process $B \to K^{(*)}\nu\overline{\nu}$ has been searched for at B factory experiments [2, 3], the sensitivity of these measurements is still far from the SM prediction for the branching fraction, leaving room for new physics contributions [4]. The challenge of these measurements lies in the fact that the $B \to K^{(*)}\nu\overline{\nu}$ decay possesses two (unobserved) neutrinos in the final state, which limits the kinematic constraints that can be used to suppress background contributions. While $B^- \to \Lambda\overline{p}\nu\overline{\nu}$ suffers from the same lack of kinematic constraints as $B \to K^{(*)}\nu\overline{\nu}$, the presence of two baryons in the final state, which can be cleanly reconstructed experimentally, provides much stronger rejection of backgrounds.

This paper presents a search for the decay $B^- \to \Lambda\overline{p}\nu\overline{\nu}$ using data recorded by the *BABAR* experiment at the PEP-II energy-asymmetric e^+e^- collider. These data were collected at the $\Upsilon(4S)$ resonance and represent an integrated luminosity of $424\,\text{fb}^{-1}$ [5], corresponding to the production of $(471 \pm 3) \times 10^6$ $B\overline{B}$ pairs [6]. This is the first time that results of a search for this process are reported. The *BABAR* detector is described in detail in Refs. [7, 8]. The charged-particle tracking system consists of a five-layer silicon vertex tracker and a 40-layer cylindrical drift chamber. Charged particle tracks are bent by a 1.5 T magnetic field produced by a superconducting solenoid, in order to enable momentum measurement. Identification of (anti)protons and other charged particles is based on measurement of the specific ionization, $\mathrm{d}E/\mathrm{d}x$, in the tracking detectors, in combination with information from the electromagnetic calorimeter and Cherenkov-photon angle information obtained from an array of fused silica quartz bars. Energy and position measurements for photons are provided by an electromagnetic calorimeter consisting of 6580 CsI(Tl) crystals arrayed as a cylindrical central barrel and a forward endcap with a conical geometry.

Simulated Monte Carlo (MC) event samples are used to develop the signal selection procedure and to estimate the selection efficiency. Studies of background channels are based on large samples of simulated events representing B^+B^- and $B^0\overline{B}^0$ production at the $\Upsilon(4S)$, and

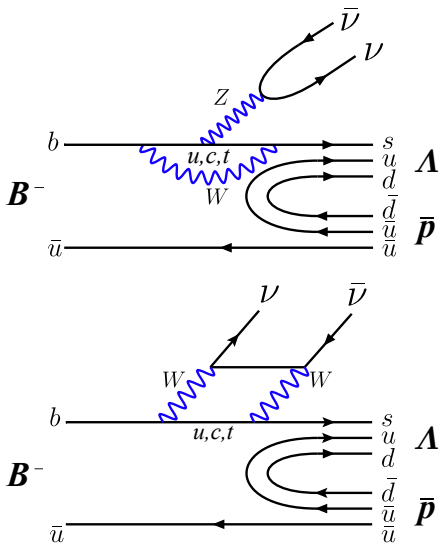

FIG. 1: Lowest order SM diagrams of the process $B^- \to \Lambda\overline{p}\nu\overline{\nu}$ in the SM. Adapted from Ref. [1].

continuum production of $e^+e^- \to q\overline{q}$ and $e^+e^- \to \tau^+\tau^-$. The $q\overline{q}$ simulation is separated into $c\overline{c}$ and light quark ($u\overline{u}, d\overline{d}, s\overline{s}$) samples. The $B\overline{B}$ samples are produced using EvtGen [9], while JETSET [10] is used for generation and hadronization of continuum background contributions, with EvtGen handling decays. For simulation of $\tau^+\tau^-$ production the KK [11] generator is used, and decays of τ leptons are simulated using the Tauola [12] package. These samples are then passed through a detector response simulation based on the GEANT4 [13] toolkit. The B^+B^-, $B^0\overline{B}^0$, and $c\overline{c}$ simulation samples correspond to an integrated luminosity which is ten times that of data, whereas the remaining continuum samples have an integrated luminosity that is four times that of data. Signal simulation for $B^- \to \Lambda\overline{p}\nu\overline{\nu}$ is generated at the $\Upsilon(4S)$ center-of-mass (CM) energy, where the B^- meson is required to decay to $B^- \to \Lambda\overline{p}\nu\overline{\nu}$, with $\Lambda \to p\pi^-$. The latter decay represents $(63.9 \pm 0.5)\%$ [14] of the Λ decay branching fraction. The B^+ is allowed to decay generically according to the measured branching fractions [14]. The signal $B^- \to \Lambda\overline{p}\nu\overline{\nu}$ process is simulated as uniformly distributed in phase space (phase space model), but this is modified at the analysis level by weighting the $m_{\Lambda\overline{p}}$ distribution according to the form factor model described in Ref. [1]. Other kinematic variables were found to have negligible impact on the signal efficiency and so were not similarly weighted; systematic uncertainties associated with the signal model are discussed later. A total of 4.053×10^6 simulated signal events are used in this analysis.

Because the decay $B^- \to \Lambda\overline{p}\nu\overline{\nu}$ has two unobserved neutrinos in the final state, it cannot be fully reconstructed. Instead, the analysis takes advantage of the

precisely known kinematics of the e^+e^- initial state and the exclusive decay $\Upsilon(4S) \to B\overline{B}$. By reconstructing the decay of one of the two B mesons, referred to as the "tag B" ($B_{\rm tag}$), into a hadronic final state, all remaining particles in the event can then be inferred to be daughters of the other B, which is referred to as the "signal B" ($B_{\rm sig}$) candidate. Moreover, the 4-vector of the $B_{\rm sig}$ can be determined independently of its decay products, from the $B_{\rm tag}$ momentum vector, $\vec{p}^{\,*}_{B_{\rm tag}}$, and the known CM energy, $E^*_{\rm CM}$: $|\vec{p}^{\,*}_{B_{\rm sig}}| = \sqrt{(E^*_{\rm CM}/2)^2 - m_B^2}$, where $\vec{p}^{\,*}_{B_{\rm sig}}$ is the three-momentum vector of the $B_{\rm sig}$, $E^*_{\rm CM}$ is the CM energy, and m_B is the B meson mass, with the direction of $\vec{p}^{\,*}_{B_{\rm sig}}$ defined to be opposite to that of $\vec{p}^{\,*}_{B_{\rm tag}}$, where the asterisks indicate quantities in the CM frame. The missing momentum four-vector, $p^*_{\rm miss}$, is determined by subtracting the CM four-momentum of all identified particles that are not used in the reconstruction of the $B_{\rm tag}$ from that of $B_{\rm sig}$. Since the $B_{\rm tag}$ has been fully reconstructed, all missing momentum in the event is attributable to the $B_{\rm sig}$ candidate. This method has been used in several previous *BABAR* analyses, for examples see Refs. [2, 16, 17].

The reconstruction of $B_{\rm tag}$ candidates considers B decays into one of a large number of possible hadronic decay modes, $B \to SX$, where S is a "seed" meson, and X is an hadronic system consisting of a combination of up to five kaons or pions with a total charge of 0 or ± 1. Although both neutral and charged $B_{\rm tag}$ candidates are reconstructed by this procedure, only $B^\pm$ candidates are retained for the current study. The seed meson can be $D^{(*)0}$, $D^{(*)\pm}$, $D_s^{*\pm}$, or J/ψ. The D meson seeds are reconstructed as: $D^+ \to K^0_S\pi^+$, $K^0_S\pi^+\pi^0$, $K^0_S\pi^+\pi^-\pi^+$, $K^-\pi^+\pi^+$, $K^-\pi^+\pi^+\pi^0$, $K^+K^-\pi^+$, and $K^+K^-\pi^+\pi^0$; $D^0 \to K^-\pi^+$, $K^-\pi^+\pi^0$, $K^-\pi^+\pi^-\pi^+$, $K^0_S\pi^+\pi^-$, $K^0_S\pi^+\pi^-\pi^0$, K^+K^-, $\pi^+\pi^-$, $\pi^+\pi^-\pi^0$, and $K^0_S\pi^0$; $D^{*+} \to D^0\pi^+$, and $D^+\pi^0$; $D^{*0} \to D^0\pi^0$, and $D^0\gamma$. The D_s^{*+} seed decay consists of $D_s^{*+} \to D_s^+\gamma$; $D_s^+ \to \phi\pi^+$, and $K^0_S K^+$. The J/ψ seed is reconstructed in the e^+e^- and $\mu^+\mu^-$ final states. In the decays above, $\pi^0 \to \gamma\gamma$, $K^0_S \to \pi^+\pi^-$, and $\phi \to K^+K^-$ are reconstructed.

A kinematic fit is then applied, which imposes vertex and nominal particle mass constraints on the selected candidates. The resulting seed candidates are then combined with kaons or pions to create $B_{\rm tag}$ candidates. Two kinematic variables are used to define these candidates:

$$m_{\rm ES} = \sqrt{(s/2 + \vec{p}_{B_{\rm tag}} \cdot \vec{p}_0)^2/E_0^2 - \vec{p}^{\,2}_{B_{\rm tag}}},$$

and $\Delta E = E^*_{\rm CM}/2 - E^*_{B_{\rm tag}}$, where E_0 and $\vec{p}_0$ are the energy and momentum of the e^+e^- system. The $B_{\rm tag}$ candidates are selected by requiring -0.12 GeV $< \Delta E <$ 0.12 GeV and 5.20 GeV/c^2 $< m_{\rm ES} <$ 5.30 GeV/c^2. If multiple candidates are present in an event, they are ranked based on reconstruction-quality criteria, in particular the value of the reconstructed seed candidate mass with respect to the nominal mass of this particle and the magnitude of ΔE. Only the best quality $B_{\rm tag}$ candidate is retained. Tagging efficiency is generally subpercent [15]. Additionally, individual $B_{\rm tag}$ modes are ranked based on the measured level of combinatorial misreconstruction, and modes with a high level of combinatorial background contributions are excluded from the analysis.

Correctly-reconstructed $B_{\rm tag}$ candidates exhibit a peak in the $m_{\rm ES}$ distribution near the B meson mass. Continuum processes and incorrectly reconstructed $B\overline{B}$ decays are referred to as "combinatorial background". The interval 5.27 GeV/c^2 $< m_{\rm ES} <$ 5.29 GeV/c^2 is defined as the signal region, while the interval between 5.20 GeV/c^2 $< m_{\rm ES} <$ 5.26 GeV/c^2 is referred to as the sideband region.

Continuum background contributions, from non-resonant $e^+e^- \to q\bar{q}$ processes, produce a combinatorial component in the $m_{\rm ES}$ distribution, including in the signal region. This background contribution is suppressed using a multivariate likelihood constructed from six global event variables. The selector is designed to discriminate comparatively more jet-like non-resonant processes from the more isotropic decay topologies of $\Upsilon(4S) \to B\overline{B}$ decays. The inputs are as follows:

- the ratio of the second and zeroth Fox-Wolfram moments [18], calculated using all reconstructed charged tracks and clusters of calorimeter energy in the event;
- the event thrust vector, the sum of the magnitudes of the momenta of all tracks and clusters projected onto the thrust axis, where the thrust axis is the axis that maximises the projection, and where the thrust vector is normalised with respect to the sum of the magnitudes of the momenta;
- the magnitude of the projection of the thrust vector onto the beam axis (z-axis);
- the cosine of the angle of the reconstructed $B_{\rm tag}$ direction with respect to the z-axis;
- the direction of the event's missing momentum vector with respect to the z-axis;
- the cosine of the angle between the thrust axes of the decay daughters of the $B_{\rm tag}$ and of the $B_{\rm sig}$.

All of these quantities are computed in the CM frame. The output of the selector, $\mathcal{L}_{B\overline{B}}$, is shown in Fig. 2 for events possessing a reconstructed $B_{\rm tag}$ with $m_{\rm ES}$ in the signal region. The $B\overline{B}$ processes peak towards $\mathcal{L}_{B\overline{B}} = 1$ while continuum processes favor values closer to zero. Events with $\mathcal{L}_{B\overline{B}} > 0.35$ are retained. This requirement rejects 76% of continuum background events and 16% of $B\overline{B}$ background events while retaining 82% of signal

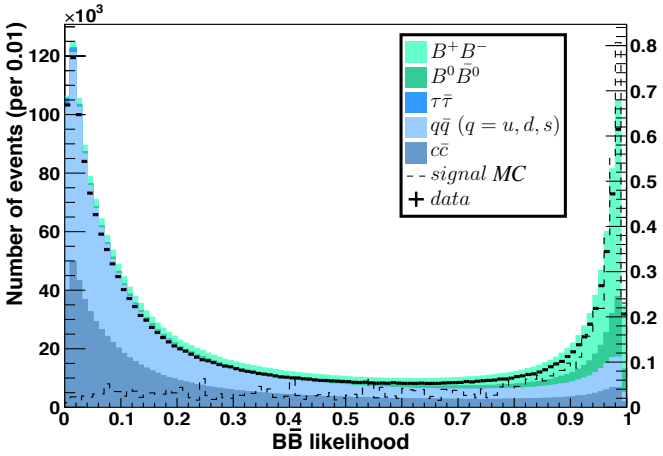

FIG. 2: Output of the $B\overline{B}$ likelihood selector, $\mathcal{L}_{B\overline{B}}$, for data (points with error bars) and background MC (stacked, shaded histograms) normalized to the data luminosity, for events with a reconstructed $B_{\rm tag}$ with 5.27 GeV/c^2 $< m_{\rm ES} <$ 5.29 GeV/c^2. The expected distribution for simulated $B^- \to \Lambda\overline{p}\nu\overline{\nu}$ events is also shown overlaid for a branching fraction of 0.4×10^{-5} (dashed line), with yields per 0.01 given by the y-axis scale on the right-hand side.

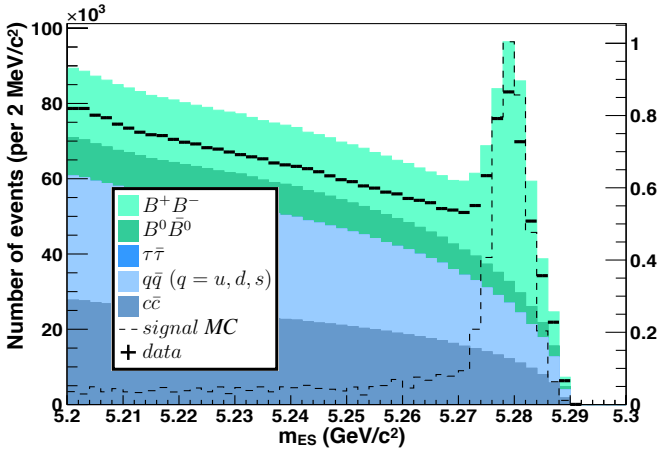

FIG. 3: The $m_{\rm ES}$ distribution for data (points with error bars) and background MC (stacked, shaded histograms) normalized to the data luminosity, for events which satisfy the continuum suppression criterion $\mathcal{L}_{B\overline{B}} > 0.35$. The expected distribution for simulated $B^- \to \Lambda\overline{p}\nu\overline{\nu}$ events is also shown overlaid for a branching fraction of 0.4×10^{-5} (dashed line), with event yields per 2 MeV/c^2 given by the y-axis scale on the right-hand side.

events. The $m_{\rm ES}$ distribution of events selected by this criterion is shown in Fig. 3.

The $B^- \to \Lambda\overline{p}\nu\overline{\nu}$ signal candidates are identified by considering all activity in the detector which is not associated with the reconstructed $B_{\rm tag}$. Since only the $\Lambda \to p\pi^-$ decay mode is considered in this analysis, $B_{\rm sig}$ candidates are required to possess exactly three charged tracks, with total charge of ± 1 opposite to that of the $B_{\rm tag}$. Signal events typically contain several low-energy clusters in the calorimeter arising from hadronic shower fragments that have not been correctly associated with reconstructed hadrons, from bremsstrahlung, or from beam-related sources. In contrast, physics background processes frequently also produce higher energy clusters attributable to daughters of π^0 decays and similar processes. To suppress these background contributions, $E_{\rm extra}$ (Fig. 4 (top)) is required to be less than 400 MeV; $E_{\rm extra}$ is the total energy of $B_{\rm sig}$ clusters where each cluster has lab-frame energy greater than 50 MeV. In events that pass this selection, these clusters are subsequently ignored.

The background MC does not accurately reproduce the event yield in data in either the signal or sideband region at this point in the selection. This deficiency has been observed in previous *BABAR* analyses [2, 16, 17] and is understood to be due to a combination of inaccurate branching fraction values and modeling of $B_{\rm tag}$ reconstruction efficiencies in the simulation. A two step procedure is applied in order to correct for these differences.

Events in the $m_{\rm ES}$ signal region can be divided into correctly reconstructed ("peaking") and combinatorial ("non-peaking") components. First, combinatorial background MC is used to estimate the combinatorial background contribution in the signal region relative to that in the sideband region; this is expressed as a ratio, $R_{\rm side}$. This is a weighted average of ratios: the ratio of each MC type's yield in the signal-region to sideband-region is calculated, then weighted according to the fraction of the total background MC in the sideband region comprising that MC type. The peaking component of B^+B^- MC in the signal region is excluded from the $R_{\rm side}$ calculation by using the $B^0\overline{B}^0$ ratio for B^+B^- events. The sideband data yield is scaled by $R_{\rm side}$ to estimate the combinatorial contribution in the $m_{\rm ES}$ signal region. As the size of the combinatorial background component depends on the relative contributions of the continuum and mis-reconstructed $B\overline{B}$ background components, the value of $R_{\rm side}$ is expected to vary depending on the signal selection criteria applied; after the signal selection described above, it is determined to have a value of $R_{\rm side} = 0.215 \pm 0.001$, where the quoted uncertainty is due to MC statistics. Systematic uncertainties related to this method are discussed below. The scaled sideband data are used to model various selection variables for the non-peaking background component in the signal region.

Second, the non-peaking background component in the signal region is combined with the subset of B^+B^- MC in the signal region in which a $B_{\rm tag}$'s reconstructed mass peaks around the known mass of a B meson; this subset of B^+B^- MC simulates the peaking contribution in the $m_{\rm ES}$ distribution. This B^+B^- peaking component is found to overestimate the $B_{\rm tag}$ yield in data, and hence is scaled by a factor $C_{\rm peak} = 0.819 \pm 0.006$ to correctly

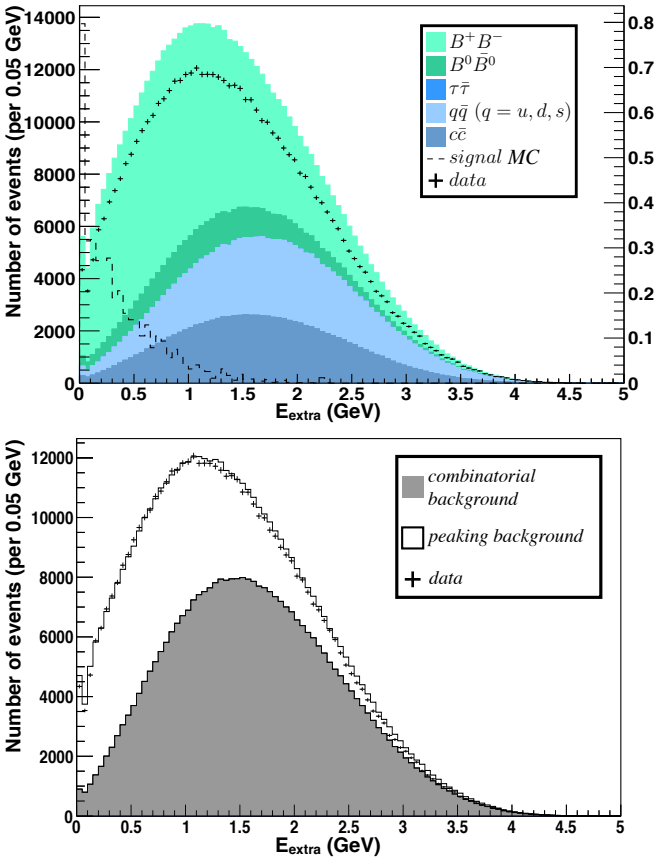

FIG. 4: Distribution of $E_{\rm extra}$, calculated in the CM frame, in data and MC before (top) and after (bottom) application of the MC correction procedure for events with a reconstructed $B_{\rm tag}$ with $m_{\rm ES}$ within the signal region. In the upper plot, data are shown as points with error bars, while background MC is shown as stacked, shaded histograms. The expected distribution for simulated $B^- \to \Lambda\bar{p}\nu\bar{\nu}$ events is shown overlaid for a branching fraction of 0.4×10^{-5} (dashed line), with yields given by the y-axis scale on the right-hand side. In the lower plot the shaded region is the sideband data scaled by $R_{\rm side}$ and the unshaded histogram is the $m_{\rm ES}$ peaking component of the B^+B^- MC scaled by $C_{\rm peak}$.

represent the data. An example of the effect of this procedure is shown in Fig. 4, which demonstrates the improved agreement between data and MC distributions after the procedure is applied.

As the quantity $C_{\rm peak}$ represents a global correction to the $B_{\rm tag}$ yield, this correction is also applied to the signal efficiency. The reconstruction efficiency for $\Upsilon(4S)$ events containing a $B^- \to \Lambda\bar{p}\nu\bar{\nu}$ decay is estimated to be approximately 0.07%, after requiring that events possess a $B_{\rm tag}$ with $m_{\rm ES}$ in the signal region and satisfy the signal selection described above. The remainder of the event selection optimization is performed "blind", i.e., without knowledge of the data yield in the signal region until the selection procedure has been finalized.

Decays of $B_{\rm sig}$ candidates are expected to contain a

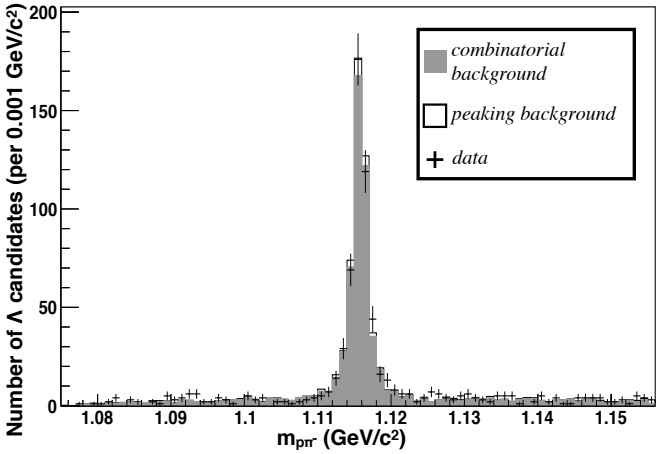

FIG. 5: The $p\pi^-$ invariant mass in events with a reconstructed $B_{\rm tag}$ with $m_{\rm ES}$ within the signal region, with three charged tracks satisfying the proton and antiproton selection and DOCA requirements. Data are shown as points with error bars, while the shaded region is the sideband data scaled by $R_{\rm side}$ and the unshaded histogram is the $m_{\rm ES}$ peaking component of the B^+B^- MC scaled by $C_{\rm peak}$.

proton-antiproton pair, and a single charged pion, where the (anti)proton with the same charge as the $B_{\rm tag}$ is presumed to be the daughter of the Λ. Tight (anti)proton particle identification criteria are applied to the baryon candidate tracks; no pion identification requirement is imposed on the third track. The (anti)proton selectors have an efficiency of 95% within the momentum range relevant to this analysis [8]. A kinematic fit is imposed on the Λ daughter tracks, applying pion and proton mass hypotheses to the tracks and fitting the Λ vertex, including a constraint that the Λ originates within a B meson flight length of the event vertex. The three tracks are also required to have a DOCA ordering consistent with a $B^- \to \Lambda\bar{p}\nu\bar{\nu}$ signal event, where DOCA is defined as the extrapolated distance of closest approach of a reconstructed track to the nominal event vertex. Due to the long mean lifetime of the Λ [14], the two $\Lambda \to p\pi^-$ decay daughters typically do not point to the interaction point, but the $\bar{p}$ that is the daughter of the $B_{\rm sig}$ does and typically has the smallest DOCA. The p that is the daughter of the Λ carries most of the Λ momentum and typically has a smaller DOCA than the π^-. This DOCA ordering requirement rejects 10% of signal events, but reduces the background rate by 24%. The resulting $p\pi^-$ invariant mass distribution, without any $\mathcal{L}_{B\bar{B}}$ or $E_{\rm extra}$ requirements imposed, is shown in Fig 5.

The Λ candidates are selected by requiring $1.112\ {\rm GeV}/c^2 < m_{p\pi^-} < 1.120\ {\rm GeV}/c^2$. If there is more than one such candidate in an event, the candidate with the highest vertex significance (the distance between the $p\pi^-$ vertex and primary event vertex, divided by its uncertainty) is selected. Following this selection,

background events within the nominal Λ mass region ($1.112\ \mathrm{GeV}/c^2 < m_{p\pi^-} < 1.120\ \mathrm{GeV}/c^2$) are almost entirely from real Λ baryons, and from $q\overline{q}$ continuum sources rather than $B\overline{B}$.

Once the Λ candidate selection is defined, a simultaneous optimization of the $\mathcal{L}_{B\overline{B}}$ and $E_{\rm extra}$ selection criteria is performed, in which the expected branching fraction limit in the absence of signal is used as the figure of merit. This optimization yields the selection criteria values presented previously. The signal efficiency is estimated to be $(0.034 \pm 0.001\ (\mathrm{stat.}))\%$.

The background yield is determined by combining the peaking background from B^+B^- MC with the combinatorial background estimated from the $m_{\rm ES}$ sideband, yielding a value of 2.3 ± 0.7 (stat.) events. The dominant contribution of 1.7 ± 0.6 (stat.) arises from combinatorial background sources.

Systematic uncertainties arise in the determination of the signal efficiency and the estimation of the background yield in the $m_{\rm ES}$ signal region. The combinatorial background yield in the $m_{\rm ES}$ signal region is determined directly from data using the method described previously. However, the shape of the combinatorial background distribution impacts the determination of the $B_{\rm tag}$ peaking yield correction and hence the peaking yield correction is anti-correlated with the sideband scaling ratio $R_{\rm side}$. Consequently, the relevant systematic uncertainty is due to the extrapolation of the observed yield of combinatoric events in the $m_{\rm ES}$ sideband to the $m_{\rm ES}$ signal region. The ratio $R_{\rm side}$ is obtained from non-peaking background MC ($q\overline{q}$, $c\overline{c}$, $\tau^+\tau^-$, $B^0\overline{B}^0$, and non-peaking B^+B^-) and its value depends on the relative mix of the continuum and $B\overline{B}$ due to the difference in shape in the predicted $m_{\rm ES}$ distributions of these two components. An uncertainty of 17% on background yield and 16% on signal efficiency is obtained by varying the shape of the $m_{\rm ES}$ distribution between that given by $B\overline{B}$ and continuum MC, and determining the impact on the resulting signal efficiency and background estimates.

The signal MC is produced using a phase-space model, which is subsequently weighted into the model of Ref. [1], based on the $m_{\Lambda\overline{p}}$ distribution. The impact of this weighting on the signal efficiency is evaluated by modifying the weighting scheme to include the other kinematic quantities $m_{\nu\overline{\nu}}$ and $\theta_{B,L}$ defined in that paper and a systematic uncertainty of 9.6% is assigned to reflect the model-dependence of the signal selection.

The remaining sources of systematic uncertainties are attributed to the MC modeling of variables used in the signal selection, and hence impact both the signal efficiency and the peaking background determinations. The impact of the 3-track requirement and the (anti)proton particle identification are evaluated using standard *BABAR* procedures [8] for the particle selectors used in this analysis, in the kinematic region that is relevant for $B^- \to \Lambda\overline{p}\nu\overline{\nu}$ decays. An uncertainty of 1.3% is assigned to the background yield estimate and 1.4% to the signal efficiency. To determine the impact of the Λ selection procedure, the Λ yield is evaluated in the $m_{\rm ES}$ sideband region, using a 4-vector sum of the p and π^- candidates to identify a Λ control sample which is independent of the kinematic fit procedure used in the nominal signal selection. The relative Λ yields determined from data and background MC, before and after applying the nominal Λ selection, are compared. The difference in relative yields for data and MC is taken as an uncertainty, resulting in a 13% correlated systematic uncertainty on both the signal efficiency and background estimate. This is associated with the DOCA ordering, kinematic fit, vertex significance, and mass selection criteria in the Λ reconstruction.

TABLE I: Summary of systematic uncertainties on the signal efficiency and backgrounds.

Source	Signal efficiency	Background
Signal weighting	9.6%	
MC modeling	16%	17%
Particle identification	1.4%	1.3%
Λ selection	13%	13%
$E_{\rm extra}$	1.9%	11%

The selection on the total energy of clusters introduces a systematic uncertainty due to the possible mismodeling of low-energy clusters in the simulation. To evaluate the impact, the cluster energies in the MC are scaled so as to precisely match the $E_{\rm extra}$ distribution in data. Parametrically, the level of data–MC agreement in the $E_{\rm extra}$ distribution (see Fig. 4) is found to be equivalent to applying a shift of 5 MeV per contributing energy cluster. The signal efficiency and background yields are then evaluated when the full signal selection is applied to samples with cluster energies shifted by ± 5 MeV. A systematic uncertainty associated with the $E_{\rm extra}$ selection criterion corresponding to the average deviation in the efficiency and background estimate is assigned, resulting in 1.9% for the signal efficiency and 11% for the background estimate. Systematic uncertainties are summarized in Table I.

The $B^- \to \Lambda\overline{p}\nu\overline{\nu}$ branching fraction is evaluated according to

$$\mathcal{B}(B^- \to \Lambda\overline{p}\nu\overline{\nu}) = \frac{N_{\rm data} - N_{\rm bg}}{\epsilon^{sig} \times N_{B^\pm}}\ , \qquad (1)$$

where $N_{\rm data}$ and $N_{\rm bg}$ are the number of events observed in data and the total estimated background yield, respectively. The overall $B^- \to \Lambda\overline{p}\nu\overline{\nu}$ signal efficiency including the $\Lambda \to p\pi^-$ branching fraction is $\epsilon^{sig} = (3.42 \pm 0.08\ (\mathrm{stat.}) \pm 0.80\ (\mathrm{sys.})) \times 10^{-4}$, and $N_{B^\pm} = (471 \pm 3) \times 10^6$ is the estimated total number of charged B mesons in the data sample [6]. It is assumed here that $\Upsilon(4S) \to B\overline{B}$ produces equal numbers of $B^0\overline{B}^0$ and

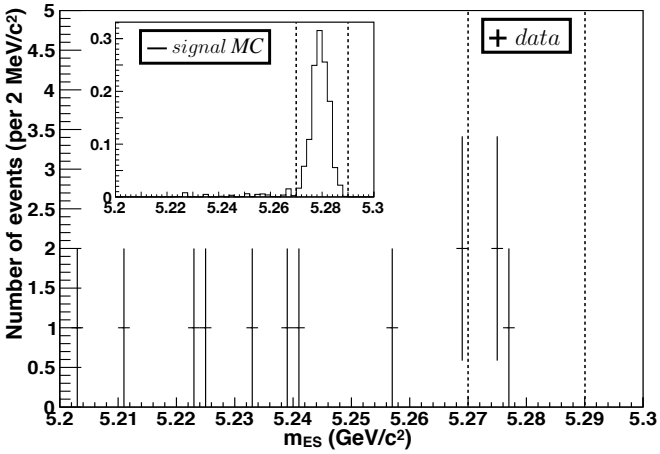

FIG. 6: The $B_{\rm tag}$ $m_{\rm ES}$ distribution of events passing all other signal selection requirements for data and for signal MC (inset) scaled to a branching fraction of $\mathcal{B}(B^- \to \Lambda\overline{p}\nu\overline{\nu}) = 0.4 \times 10^{-5}$. The signal region is indicated by the vertical dashed lines, and the total background expected in the signal region is 2.3 ± 0.7 (stat.) ± 0.6 (sys.) events.

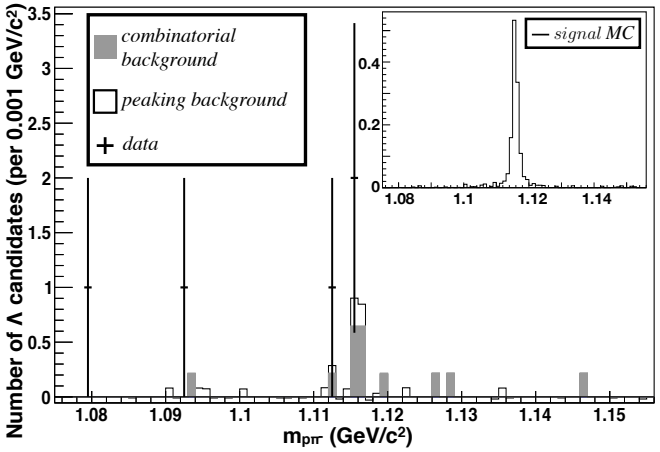

FIG. 7: The $p\pi^-$ invariant mass in events passing all other signal selection requirements. Data are shown as points with error bars, while the background expectation is shown as solid histograms. The negative bin values are a consequence of the background estimation procedure applied to low-statistics histograms. The expected signal distribution from MC is shown in the inset histogram, and is scaled to a branching fraction of $\mathcal{B}(B^- \to \Lambda\overline{p}\nu\overline{\nu}) = 0.4 \times 10^{-5}$.

B^+B^- pairs.

When the full selection is applied to the data sample, a total of $N_{\rm data} = 3$ events are found in the $m_{\rm ES}$ signal region, consistent with the background yield expectation of $N_{\rm bg} = 2.3 \pm 0.7$ (stat.) ± 0.6 (sys.). The $m_{\rm ES}$ distribution of the $B_{\rm tag}$ in events that pass all other selection requirements is plotted in Fig. 6, and the $p\pi^-$ invariant mass distribution is shown in Fig. 7. The central value of the branching fraction is determined to be $\mathcal{B}(B^- \to \Lambda\overline{p}\nu\overline{\nu}) = (0.4 \pm 1.1\ (\text{stat.}) \pm 0.6\ (\text{sys.})) \times 10^{-5}$. As no evidence is found for signal, a 90% confidence level upper limit is computed using the Barlow method [19], yielding $\mathcal{B}(B^- \to \Lambda\overline{p}\nu\overline{\nu}) < 3.0 \times 10^{-5}$.

In signal MC we observe no significant correlation between signal efficiency and q^2, the square of the four-momentum transfer to the $\nu\overline{\nu}$ pair.

A comparison of the branching fraction limit and its SM-predicted value allows us to place a constraint on beyond-SM values of $|C_L^\nu|$, the Wilson coefficient that describes left-handed weak currents. Using the parametrization of Ref. [20], and assuming the SM value of $C_R^\nu = 0$ (that is, there are no right-handed weak currents), we can place an upper limit on $\epsilon = |C_L^\nu|/|(C_L^\nu)^{\rm SM}|$ of 7.4 at the 90% confidence level. The same calculation for the related $b \to s\nu\overline{\nu}$ modes $B \to K^{(*)}\nu\overline{\nu}$, using measured and predicted branching fraction values from Refs. [2, 3, 21], yields upper limits on ϵ of 2.2 for $B^+ \to K^+\nu\overline{\nu}$ and 2.7 for $B^0 \to K^{*0}\nu\overline{\nu}$ at the 90% confidence level.

In conclusion, a search has been performed for the FCNC decay process $B^- \to \Lambda\overline{p}\nu\overline{\nu}$ based on the full *BABAR* dataset collected at the CM energy of the $\Upsilon(4S)$ resonance. No evidence is found for an excess over the SM prediction and we report the first branching fraction limit on this decay.

ACKNOWLEDGMENTS

The authors gratefully acknowledge David M. Straub's help in determining the new physics implications of this analysis. We are grateful for the excellent luminosity and machine conditions provided by our PEP-II colleagues, and for the substantial dedicated effort from the computing organizations that support *BABAR*. The collaborating institutions wish to thank SLAC for its support and kind hospitality. This work is supported by DOE and NSF (USA), NSERC (Canada), CEA and CNRS-IN2P3 (France), BMBF and DFG (Germany), INFN (Italy), FOM (The Netherlands), NFR (Norway), MES (Russia), MICIIN (Spain), STFC (United Kingdom). Individuals have received support from the Marie Curie EIF (European Union), the A. P. Sloan Foundation (USA), and the Binational Science Foundation (USA-Israel).

* Now at: Wuhan University, Wuhan 430072, China
† Now at: Università di Bologna and INFN Sezione di Bologna, I-47921 Rimini, Italy
‡ Deceased
§ Now at: University of Huddersfield, Huddersfield HD1 3DH, UK
¶ Now at: University of South Alabama, Mobile, Alabama 36688, USA

** Also at: Università di Sassari, I-07100 Sassari, Italy
†† Also at: Gran Sasso Science Institute, I-67100 LAquila, Italy

[1] C. Q. Geng and Y. K. Hsiao, Phys. Rev. D **85**, 094019 (2012).
[2] J. P. Lees *et al.* [*BABAR* Collaboration], Phys. Rev. D **87**, 112005 (2013).
[3] O. Lutz *et al.* [BELLE Collaboration], Phys. Rev. D **87** 111103 (2013).
[4] F. Sala and D. M. Straub, Phys. Lett. B **774**, 205 (2017).
[5] J. P. Lees *et al.* [*BABAR* Collaboration], Nucl. Instrum. Meth. A **726**, 203 (2013).
[6] A. J. Bevan, B. Golob, T. Mannel *et al.*, Eur. Phys. J. C **74**, 3026 (2014).
[7] B. Aubert *et al.* [*BABAR* Collaboration], Nucl. Instrum. Meth. A **479**, 1 (2002).
[8] B. Aubert *et al.* [*BABAR* Collaboration], Nucl. Instrum. Meth. A **729**, 615 (2013).
[9] D. J. Lange, Nucl. Instrum. Meth. A **462**, 152 (2001).
[10] T. Sjöstrand, Comp. Phys. Commun. **82**, 74 (1994).
[11] S. Jadach, B. F. L. Ward, and Z. Wąs, Comp. Phys. Commun. **130**, 260 (2000).
[12] S. Jadach *et al.*, Comput. Phys. Commun. **76**, 361 (1993).
[13] S. Agostinelli *et al.* [GEANT4 Collaboration], Nucl. Instrum. Meth. A **506**, 250 (2003).
[14] M. Tanabashi *et al.* [Particle Data Group], Phys. Rev. D **98**, 030001 (2018).
[15] A. J. Bevan, B. Golob, T. Mannel *et al.*. Eur. Phys. J. C **74**, 3026 (2014).
[16] J. P. Lees *et al.* [*BABAR* Collaboration], Phys. Rev. Lett. **118**, 031802 (2017).
[17] B. Aubert *et al* [*BABAR* collaboration], Phys. Rev. D **80**, 111105 (2009).
[18] G. C. Fox and S. Wolfram, Nucl. Phys. B **149**, 413 (1979).
[19] R. Barlow, Comput. Phys. Comm. **149**, 97 (2002).
[20] W. Altmannshofer *et al.*, J. High Energy Phys. **04**, 022 (2009).
[21] A. J. Buras *et al.*, J. High Energy Phys. **02**, 184 (2015).